Available online at www.sciencedirect.com
ScienceDirect
International Journal of Heat and Fluid Flow 28 (2007) 454–468
International Journal of HEAT AND FLUID FLOW
www.elsevier.com/locate/ijhff

Mixed convection heat transfer to and from a horizontal cylinder in cross-flow with heating from below

G.M. Laskowski [a,*], S.P. Kearney [b], G. Evans [a], R. Greif [c]

[a] Sandia National Laboratories[1], P.O. Box 969, Livermore, CA 94551, USA
[b] Sandia National Laboratories, P.O. Box 5800, Albuquerque, NM 87185, USA
[c] Department of Mechanical Engineering, University of California, Berkeley, CA 94720, USA

Received 12 February 2006; received in revised form 31 March 2006; accepted 10 May 2006
Available online 17 July 2006

Abstract

Heat transfer to and from a circular cylinder in a cross-flow of water at low Reynolds number was studied both experimentally and numerically. The experiments were carried out in a high aspect ratio water channel. The test section inflow temperature and velocity, channel lower surface temperature and cylinder surface temperature were controlled to yield either laminar or turbulent flow for a desired Richardson number. When the lower surface was unheated, the temperatures of the lower surface and water upstream of the cylinder were maintained approximately equal and the flow was laminar. When the lower surface was heated, turbulence intensities as high as 20% were measured several cylinder diameters upstream of the cylinder due to turbulent thermal plumes produced by heating the lower surface. Variable property, two-dimensional simulations were undertaken using a variant of the v^2–f turbulence model with buoyancy production of turbulence accounted for by a simple gradient diffusion model. Predicted and measured heat flux distributions around the cylinder are compared for values of the Richardson number, Gr_d/Re_d^2, from 0.3 to 9.3. For laminar flow, the predicted and measured heat flux results agreed to within the experimental uncertainty. When the lower surface was heated, and the flow was turbulent, there was qualitative agreement between predicted and measured heat flux distributions around the cylinder. However the predicted spatially averaged Nusselt number was from 37% to 53% larger than the measured spatially averaged Nusselt number. Additionally, spatially averaged Nusselt numbers are compared to correlations in the literature for mixed convection heat transfer to/from cylinders in cross-flow. The results presented here are larger than the correlation values. This is believed to be due to the effects of buoyancy-induced turbulence resulting from heating the lower surface and the proximity of the cylinder to that surface.

Keywords: Buoyant turbulence; Mixed convection; Cylinder; Cross-flow

1. Introduction

There are many important applications (e.g., heat transfer in fires; materials processing; electronic equipment cooling; nuclear reactor cooling) of convective heat transfer in the mixed convection regime, defined typically as the regime where the heat transfer differs by more than 5% from either pure forced convection or pure natural convection (Fand and Keswani, 1973; Siebers et al., 1982). Most theoretical and experimental studies of turbulent mixed convection heat transfer have been carried out in relatively simple configurations, some of which are summarized in Table 1.

An interesting result found in much of the above cited work is that when the forced flow is aiding the natural convection flow such as occurs in a forced upflow in a heated tube or adjacent to a heated vertical flat plate or a heated vertical backward facing step, the turbulent mixed convection regime results in reduced heat transfer compared with

* Corresponding author. Fax: +1 518 387 6126.
E-mail address: laskowsk@research.ge.com (G.M. Laskowski).
[1] Sandia is a multiprogram laboratory operated by Sandia Corporation, a Lockheed-Martin Company, for the United States Department of Energy's National Nuclear Security Administration under Contract DE-AC04-94AL85000.

0142-727X/$ - see front matter © 2006 Elsevier Inc. All rights reserved.
doi:10.1016/j.ijheatfluidflow.2006.05.004

Nomenclature

c_p	specific heat
CW	clockwise direction
d	cylinder diameter = 1.5875 cm
f	Helmholtz function (turbulence model)
g	acceleration of gravity
G	turbulence production due to buoyancy
Gr_d	Grashof number based on $d = (g\beta_f\lvert\overline{T}_{cyl} - \overline{T}_{in}\rvert d^3)/\nu_f^2$
Gr_l	Grashof number based on $l = (g\beta_f\lvert\overline{T}_w - \overline{T}_{in}\rvert l^3)/\nu_f^2$
Gr_x	Grashof number based on $x = (g\beta_f\lvert\overline{T}_w - \overline{T}_{in}\rvert x^3)/\nu_f^2$
h	heat transfer coefficient $= q/\lvert(\overline{T}_{cyl} - \overline{T}_{in})\rvert$
H	channel height = 7.62 cm
k	thermal conductivity, turbulent kinetic energy
l	length of heated section to cylinder axis = 42 cm
L	turbulent length scale, length of test section
n	normal vector
nd	non-dimensional
Nu	Nusselt number $= hd/k$
p	pressure
P	turbulence production due to shear
Pr	Prandtl number $= \mu C_p/k$
q	time averaged heat flux $= \frac{1}{t^*}\int_0^{t^*} k_{eff}\nabla T\cdot\hat{n}\Big\rvert_{cyl} dt$
Ra_d	Rayleigh number $= Gr_d Pr$
Re_d	Reynolds number based on $d = \overline{U}_{in} d/\nu_f$
Re_x	Reynolds number based on $x = \overline{U}_{in} x/\nu_f$
Ri_d	Richardson number $= Gr_d/Re_d^2$
t	time
T	temperature, turbulent time scale
T_f	film temperature $= (\overline{T}_{in} + \overline{T}_{cyl})/2$
TI	turbulence intensity
TL	turbulent length scale
$u_{i,j,k}$	velocity component
u	streamwise component of velocity
v	wall normal component of velocity
v^2	wall normal variance (turbulence model)
V	volume
w	spanwise component of velocity
x, y, z	coordinate direction
β	coefficient of thermal expansion $= -1/\rho(\partial\rho/\partial T)$
δ_{ij}	Kronecker delta
ε	turbulent dissipation
κ	von Karman constant = 0.41
μ	dynamic viscosity
ν	kinematic viscosity $= \mu/\rho$
θ	angular measure
ρ	density
σ	turbulence closure coefficient
τ	shear stress

Subscripts

cyl	cylinder value
d	cylinder diameter value
f	film temperature value
in	inflow value
lam	laminar
turb	turbulent
w	lower wall value

the limiting cases of either forced or natural convection. For example, in an experimental study of turbulent mixed convection from a heated vertical flat plate to an upward flow of water, Kitamura and Inagaki (1987) showed a reduction in the Nusselt number of up to 25% below the limiting values for forced or natural convection. In experimental studies of the effects of forced flow on the turbulent natural convection boundary layer on a heated vertical surface, Hattori et al. (2000, 2001) and Abu-Mulaweh et al. (2000) showed that the reduction in heat transfer is related to the delay of transition and laminarization of the boundary layer with increasing free-stream velocity.

Extensive literature exists on heat transfer from cylinders in cross-flow including a review by Morgan (1975) and the book of and Zhukauskas and Ziugzda (1985). Fand and Keswani (1973) studied mixed convection from heated horizontal cylinders in water subject to a cross-flow. For $0.5 < Gr_d/Re_d^2 < 2$ they correlated average Nusselt number results as a buoyancy correction to the forced convection result. For $Gr_d/Re_d^2 > 40$ their correlation was in

Table 1
Studies of turbulent mixed convection

Case	Reference
Vertical plate flow (2D)	Lin and Churchill (1978), Kitamura and Inagaki (1987), Chen et al. (1987), Patel et al. (1998), Abu-Mulaweh et al. (2000), Hattori et al. (2000, 2001)
Vertical plate flow (3D)	Siebers et al. (1982), Plumb and Evans (1983), Afshari (1989), Evans et al. (2005)
Upflow and downflow in vertical tubes	Abdelmeguid and Spalding (1979); review by Jackson et al. (1989), Joye et al. (1989), Cotton and Jackson (1990), Aicher and Martin (1997)
Flow over horizontal plate	Imura et al. (1978), Cheng et al. (1986), Ramachandran et al. (1990)
Vertical backward facing step	Li et al. (1998), Abu-Mulaweh et al. (2001)
Cavity flow	Humphrey and To (1986)

terms of an equivalent Reynolds number for the buoyant flow with the combined forced and buoyant effects included as a vectorial sum. For the intermediate region with $2 < Gr_d/Re_d^2 < 40$ they reported unsteady heat transfer but did not give a correlation. Their results are applicable for $200 < Re_d < 1500$ and $5 \times 10^4 < Gr_d < 4.0 \times 10^6$. Oosthuizen and Madan (1970) studied mixed convection from heated cylinders in air in an aiding flow geometry. Their results for the average Nusselt number were correlated in terms of Gr_d/Re_d^2 and apply for $100 < Re_d < 3000$ and $2.5 \times 10^4 < Gr_d < 3.0 \times 10^5$. They found that the Nusselt number was within 5% of the forced convection value for $Gr_d/Re_d^2 < 0.28$. In an experimental study of forced convection heat transfer from a heated cylinder to a cross-flow of air, Lowery and Vachon (1975) found that increased turbulence intensity in the free-stream up to 14% resulted in increased heat transfer up to 60% in the stagnation region and in the laminar boundary layer (up to 40° from the stagnation point). However, the overall cylinder heat transfer was shown to either increase or decrease, depending on turbulence intensity and Reynolds number, due to the decrease in heat transfer in the separated region with increasing turbulence intensity. Their study was for $1.09 \times 10^5 < Re_d < 3.02 \times 10^5$ which is significantly larger than the Reynolds numbers studied here. In a numerical study of aiding laminar mixed convection past a heated horizontal cylinder in air, Chang and Sa (1989) found critical values of Gr_d/Re_d^2 (0.15 for $Re_d = 100$; 0.5 for $Re_d = 200$), above which the cylinder heat transfer decreased as Gr_d/Re_d^2 was increased. The decrease in heat transfer with increasing Gr_d/Re_d^2 was temporary, eventually increasing with further increases in Gr_d/Re_d^2. They showed that the decrease in heat transfer was due to a change of flow pattern in the wake where unsteady vortices were replaced with stationary recirculation regions. Clearly, mixed convection heat transfer to or from a cylinder is a complex phenomenon.

The present study is concerned with heat transfer to/from a cooled/heated cylinder in a cross-flow of water (cf. Fig. 1) which was examined both experimentally and numerically. The work is motivated by the need to predict heat transfer to and from objects in fire environments in both the forced and mixed convection regimes. While the primary heat transfer mechanism in such environments is radiation, turbulent convection can account for as much as 20% of the overall heat transfer (Nakos and Keltner, 1989). Furthermore, the magnitude and distribution of the radiation component of the heat transfer resulting from

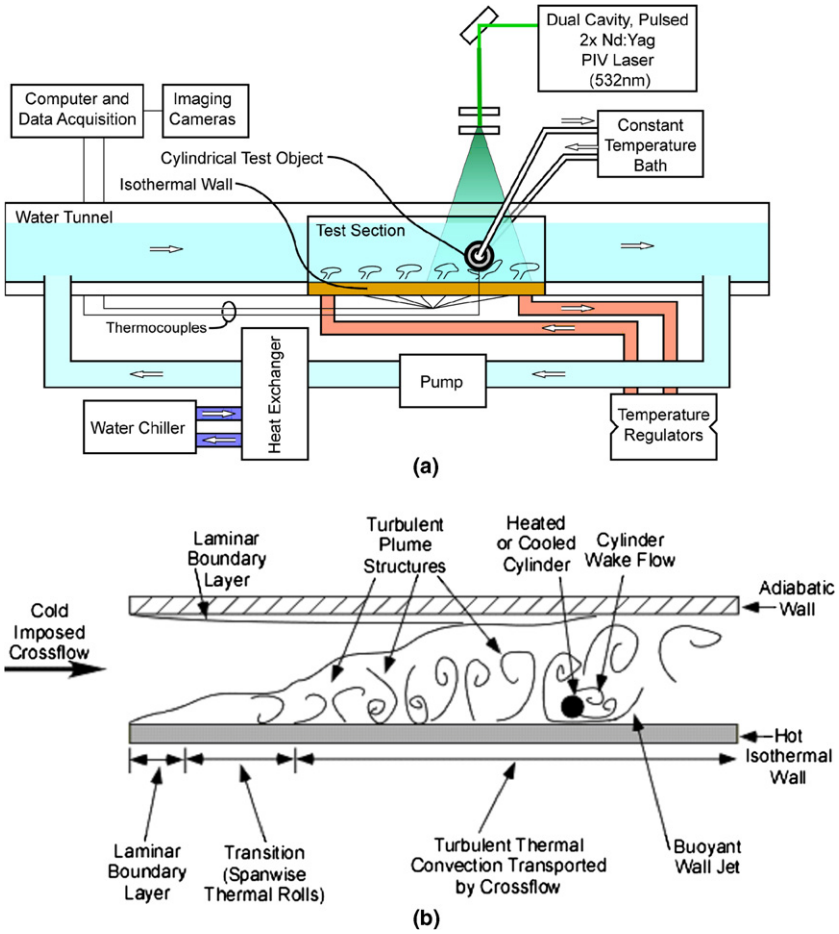

Fig. 1. (a) Schematic of water channel and (b) cartoon of flow physics in the test section for lower heated surface cases.

combustion of fuel depends strongly on the flow field and turbulence structure and intensity. Hence, the ability to predict radiative heat transfer depends on the ability to predict or simulate the turbulent flowfield. This study is intended to quantify convective heat transfer to/from a cylindrical object in both the laminar and turbulent mixed convection regimes in the absence of combustion and radiation. Water was chosen as the working fluid to approximate the dimensionless flow parameters, Re_d and $Ri_d = Gr_d/Re_d^2$, for heat transfer to/from an object in a pool fire environment while maintaining a relatively small-scale experiment. The cases investigated in the current study are summarized in Table 2.

In all cases studied the water flow at the entrance to the test section ($x = 0$) was laminar. When the lower surface of the channel in the test section ($0 \leqslant x \leqslant 61$ cm) was maintained at approximately the same temperature as the water entering the test section, as in cases 1 and 2, the flow was laminar from $x = 0$ to the cylinder located at $x = 42.7$ cm (cf. Fig. 1). However, when the lower surface of the channel in the test section was heated, as in cases 3 and 4, the flow was turbulent with thermal plumes rising from almost the entire heated lower surface of the test section. In previous experimental studies of the flow of water over a heated horizontal surface (Cheng et al., 1986; Imura et al., 1978) it was found that for $Gr_x/Re_x^{3/2} > 100$, where x is the distance from the leading edge of the heated horizontal surface, the laminar flow became unstable and consisted of longitudinal vortical structures, and for $Gr_x/Re_x^{3/2} > 300$ the flow consisted of turbulent thermal plumes and the heat transfer from the lower surface was essentially turbulent free convection. For case 3 in Table 2 of the present study, $Gr_x/Re_x^{3/2} > 300$ for $x > 6$ cm, which is only 14% of the distance in the x direction from the start of the heated section to the location of the cylinder. In addition to three-dimensional effects due to heating of the lower channel surface, it is widely recognized that flow past an adiabatic or isothermal circular cylinder is largely three-dimensional as well (see for example Williamson, 1996; Kieft et al., 1999; Lei et al., 2001; van Steenhoven and Rindt, 2003). While the flow under investigation can be categorized as three-dimensional, the experiment was designed to minimize these effects and measurements were conducted that verified the two-dimensionality of the cylinder heat transfer. Since the primary quantity of interest in this study is the cylinder heat transfer, two-dimensional simulations were conducted.

2. Description of the water channel facility

The purpose of the experiment was to measure two metrics, namely the flowfield near the cylinder as well as the heat flux to/from the cylinder. The velocity field was measured using a standard 2D digital PIV system, details of which are discussed elsewhere (Kearney et al., 2005). The focus of this paper is the cylinder surface heat flux and the details of those measurements will be outlined following the discussion of the water channel facility shown schematically in Fig. 1.

Water flows from a settling chamber through flow conditioning honeycomb and screens to a two-dimensional contraction and into a test section with a heated, isothermal lower surface. The water layer depth is 76 mm and the width of the test section is 610 mm, which results in a flowfield aspect ratio of 8 that should yield nominally two-dimensional flow and heat-transfer statistics near the spanwise center of the test section. The heated lower surface of the test section is 610 mm × 610 mm in the spanwise and streamwise directions. This surface consists of two thermally massive copper plates brazed together. Headers and serpentine channels milled into one of the copper plates before brazing form a distribution network for controlled-temperature hot water which supplied heat to the surface. Forty-five T-type thermocouples were inserted through holes in the thick portions of the copper wall to within 500 μm of the upper copper surface. These thermocouples indicated a temperature nonuniformity of ±0.25 °C, which was only 0.7–1.3% of the temperature differences driving the turbulent convection, so that the lower surface of the water channel can be considered to be isothermal. A thermally thin black-anodized aluminum sheet was bonded to the copper wall using a common heat-sink compound. The anodized sheet was added to the facility to minimize scattered laser light from the test-section wall, which was hampering the PIV measurements. The test section was capped with a 19-mm thick acrylic lid, which provides an approximately adiabatic upper boundary. Energy input to the flowfield was removed by circulating the flow

Table 2
Experimental conditions

	Case description	$\overline{U}_{in}$ (cm/s)	$\overline{T}_{in}$ (K)	$\overline{T}_{cyl}$ (K)	$\overline{T}_w$ (K)	Re_d	Gr_d	Ri_d	Gr_l
Unheated lower surface	Case 1 Laminar forced	1.75	291.4	286.7	291.4	251	2.5×10^4	0.4	0
	Case 2 Laminar mixed	1.09	284.1	311.5	284.1	192	3.4×10^5	9.1	0
Heated lower surface	Case 3 Turbulent forced	1.75	290.0	286.6	318.0	246	1.6×10^4	0.3	5×10^9
	Case 4 Turbulent mixed	1.09	284.0	311.3	318.0	189	3.3×10^5	9.3	8×10^9

facility water through a stainless-steel water-to-water heat exchanger that was supplied with controlled-temperature chilled water. In this fashion, the approach flow temperature field was well controlled.

A 15.9-mm ($d/H = 0.21$) diameter thick-walled stainless-steel tube spanned the test section at a streamwise distance of 427 mm ($x/L = 0.7$) from the beginning of the heated section. The cylinder's axis was positioned 14.3 mm ($y_0/H = 0.19$) above the test-section floor. In the case of the heated lower surface, temperature fluctuation spectra obtained from preliminary flowfield measurements using 36-gauge T-type thermocouple rakes showed that the wall-normal height of the cylinder axis was approximately at the edge of the time-mean thermal boundary layer on the heated lower surface. Spatially resolved time-mean heat flux measurements were performed at the spanwise centerline of the test cylinder. These heat flux data served as the primary code validation metric and were performed by converting measured cylinder surface temperatures to heat fluxes via the solution of a well-posed 2D conduction problem for the annular domain between the outer and inner surfaces of the test cylinder.

2.1. Spatially resolved heat flux measurements

The time-mean heat flux around the outer circumference of the test cylinder was resolved and used as a primary code-validation metric. A detail of the stainless-steel test cylinder used for these measurements is provided in Fig. 2. The temperature profile around the circumference of the cylinder was measured near the spanwise center of the water channel test section. Cooled or heated water flowing inside the cylinder was used to control the magnitude of the outer surface temperature. Heat flux data were inferred from the solution of a well-posed 2D conduction problem on the annular domain of the stainless-steel cylinder, subject to experimentally obtained boundary conditions at the inner and outer surfaces. Details of the conduction solution are provided in Appendix A. The boundary condition at the outer surface of the cylinder was the measured circumferential temperature profile. A mixed convective–conductive condition was used at the inner surface, where the convection coefficient was computed from the Dittus and Boelter (1930) correlation using the metered flow rate and temperature of the water flowing through the cylinder as inputs.

The outer surface of the cylinder was instrumented with 36-gauge T-type thermocouples that were potted with a conductive epoxy into 0.89-mm square axial grooves machined into the 4.76-mm thick cylinder wall. The grooves were initiated at the axial edges of the cylinder, which were external to the water channel test section, and terminated 6.35 mm from the cylinder spanwise centerline. There were 13 axial grooves in total with the grooves machined in two "sets" emanating from different spanwise ends. The thermocouples in each set were separated by 60° and the two sets were staggered by 30°. Cylinder outer surface temperature measurements were recorded by averaging the thermocouple data for nominally 2 min and then rotating the cylinder in 15° increments to span a ±75° range. In this manner, an ensemble of surface temperature measurements with 15° resolution around the outer cylinder circumference was obtained. The averaged temperatures at each location were the result of readings from as many as 11 different thermocouples so that sensor-to-sensor bias in the measurement was minimized. The total data averaging period at each location was approximately 20 min, which was of order 10^3 integral time scales of the thermal structures produced in the flow as a result of heating the lower surface of the channel. The convective boundary condition at the inner surface of the cylinder was obtained from rotameter readings with ±0.1 GPM resolution and from thermocouple measurements of the temperature of the water flowing through the cylinder. The total

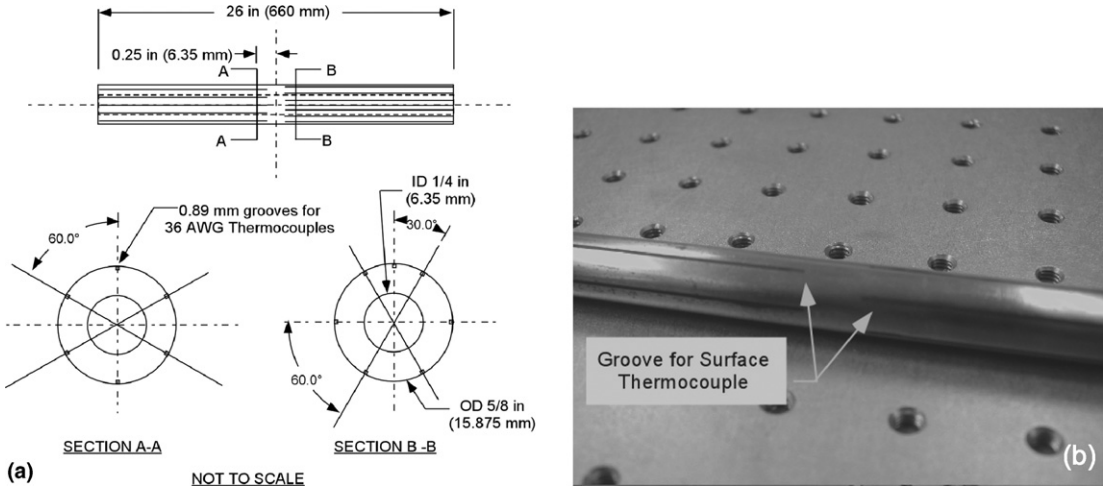

Fig. 2. Test cylinder for convection experiments (a) an engineering drawing of the cylinder design and (b) a close-up of the cylinder showing the epoxied thermocouple grooves.

temperature rise of this water was no larger than 1.5 °C. This procedure results in a heat-flux measurement with an estimated ±15% systematic (bias) error and ±5–7% precision (scatter) error.

3. Description of the numerical method

The numerical simulations were conducted with SIERRA/Fuego (Moen et al., 2002), a parallel, three-dimensional, transient, unstructured, variable-property, low Mach number Reynolds Averaged Navier–Stokes (RANS) code. Although not utilized here, Fuego also supports conjugate heat transfer and combustion capabilities and, when coupled with other codes in the SIERRA framework, allows for large-scale fire simulations. Both hexahedral and tetrahedral unstructured meshes can be used; only hexahedral elements are used for the present simulations.

3.1. Governing and model equations

The low Mach number RANS equations are written and solved in integral form:

$$\text{Mass} \quad \int \frac{\partial \rho}{\partial t} \mathrm{d}V + \int \rho u_j n_j \,\mathrm{d}S = 0 \tag{1a}$$

$$\text{Momentum} \quad \int \frac{\partial \rho u_i}{\partial t} \mathrm{d}V + \int (\rho u_i u_j) n_j \,\mathrm{d}S = \int (-p\delta_{ij}) n_j \,\mathrm{d}S + \int \mu_{\text{eff}} \left(\frac{\partial u_i}{\partial x_j} + \frac{\partial u_j}{\partial x_i} \right) n_j \,\mathrm{d}S + \int (\rho - \rho_\infty) g_i \,\mathrm{d}V \tag{1b}$$

$$\text{Energy} \quad \int \frac{\partial \rho h}{\partial t} \mathrm{d}V + \int (\rho h u_j) n_j \,\mathrm{d}S = \int \frac{k_{\text{eff}}}{C_p} \frac{\partial h}{\partial x_j} n_j \,\mathrm{d}S \tag{1c}$$

where $\mu_{\text{eff}} = \mu_{\text{lam}}(T) + \mu_{\text{turb}}$ and $k_{\text{eff}} = k_{\text{lam}}(T) + k_{\text{turb}}$. The turbulent viscosity and thermal conductivity are computed using a segregated version of Durbin's (1991) v^2–f model described by Kalitzin (1999). In addition, modifications to the treatment of the turbulent time scale suggested by Sveningsson (2003) to aid in stability were implemented. A simplified gradient diffusion hypothesis (SGDH) (Rodi and Hossain, 1982) term is included to account for production of turbulent kinetic energy due to thermal buoyancy. The model computes an isotropic turbulent viscosity $\mu_{\text{turb}} = c_\mu \rho \overline{v^2} T$ where:

$$\int \frac{\partial \rho k}{\partial t} \mathrm{d}V + \int (\rho k u_j) n_j \,\mathrm{d}S = \underbrace{\int (P_k + G_k) \,\mathrm{d}V}_{\text{production of } k} - \underbrace{\int (\rho \varepsilon) \,\mathrm{d}V}_{\text{dissipation of } k} + \underbrace{\int \left[\left(\mu_{\text{lam}} + \frac{\mu_{\text{turb}}}{\sigma_k} \right) \frac{\partial k}{\partial x_j} \right] n_j \,\mathrm{d}S}_{\text{diffusion}}$$

$$\int \frac{\partial \rho \varepsilon}{\partial t} \mathrm{d}V + \int (\rho \varepsilon u_j) n_j \,\mathrm{d}S = \underbrace{\int c_{\varepsilon_1} (P_k + c_{\varepsilon_G} G_k) \frac{1}{T} \mathrm{d}V}_{\text{production of } \varepsilon} - \underbrace{\int c_{\varepsilon_2} \left(\rho \varepsilon \frac{1}{T} \right) \mathrm{d}V}_{\text{dissipation of } \varepsilon} + \underbrace{\int \left[\left(\mu_{\text{lam}} + \frac{\mu_{\text{turb}}}{\sigma_\varepsilon} \right) \frac{\partial \varepsilon}{\partial x_j} \right] n_j \,\mathrm{d}S}_{\text{diffusion}}$$

$$\int \frac{\partial \rho \overline{v^2}}{\partial t} \mathrm{d}V + \int (\rho \overline{v^2} u_j) n_j \,\mathrm{d}S = \underbrace{\int (\rho k f) \,\mathrm{d}V}_{\text{production of } \overline{v^2}} - \underbrace{\int \left(\frac{N \overline{v^2}}{T_1} \right) \mathrm{d}V}_{\text{dissipation of } \overline{v^2}} + \underbrace{\int \left[\left(\mu_{\text{lam}} + \frac{\mu_{\text{turb}}}{\sigma_{\overline{v^2}}} \right) \frac{\partial \overline{v^2}}{\partial x_j} \right] n_j \,\mathrm{d}S}_{\text{diffusion}}$$

$$\int \frac{f}{L^2} \mathrm{d}V - \int \frac{\partial f}{\partial x_j} n_j \,\mathrm{d}S = \int \frac{c_2}{L^2} \left(\frac{P_k + G_k}{\rho k} \right) \mathrm{d}V + \int \frac{c_1}{L^2} \left(\frac{2/3 - \overline{v^2}/k}{T_1} \right) \mathrm{d}V + \int \frac{(N-1)}{L^2} \frac{\overline{v^2}/k}{T_1} \mathrm{d}V \tag{2}$$

and the production terms, time and length scales are defined as:

$$P_k = 2\mu_{\text{turb}} S_{ij} S_{ij} \quad G_k = \rho \beta \frac{\nu_{\text{turb}}}{Pr_{\text{turb}}} g_j \frac{\partial T}{\partial x_j}$$

$$T = \min \left[T_1, \frac{\alpha k}{2\sqrt{3\overline{v^2}} c_\mu |S|} \right] \quad T_1 = \max \left(\frac{k}{\varepsilon}, 6\sqrt{\frac{\nu}{\varepsilon}} \right)$$

$$L = c_L \max \left(\frac{k^{3/2}}{\varepsilon}, c_\eta \left(\frac{\nu^3}{\varepsilon} \right)^{1/4} \right) \quad S_{ij} = \frac{1}{2} \left(\frac{\partial u_i}{\partial x_j} + \frac{\partial u_j}{\partial x_i} \right) \quad |S| = \sqrt{S_{ij} S_{ij}} \tag{3}$$

where $\beta = \beta(T)$. The turbulent thermal conductivity is assumed to be isotropic and is based on a constant turbulent Prandtl number assumption, $Pr_{\text{turb}} = C_p \mu_{\text{turb}} / k_{\text{turb}}$ and was initially set to 0.9. The closure coefficients for the v^2–f model are listed in Table 3.

Eqs. (1)–(3) are solved via a segregated projection method loosely based on the control volume finite element method (CVFEM) algorithm of Baliga and Patankar (1983) and Schneider and Raw (1986). Evans et al. (2005) successfully applied a variant of this code in the study of turbulent mixed convection from a high temperature vertical flat plate.

3.2. Code verification

Several verification cases were undertaken to demonstrate that the numerical algorithms and models in Fuego functioned correctly. The first case, turbulent isothermal channel flow ($Re_\tau = 180$), demonstrated that the v^2–f model correctly predicted the mean flow and turbulence quantities

Table 3
Closure coefficients for the v^2–f model

c_μ	c_{ε_1}	c_{ε_2}	c_{ε_G}	σ_k	σ_ε	$\sigma_{\overline{v^2}}$	c_1	c_2	c_L	c_η	N
0.22	1.4	1.9	1.0	1.0	1.3	1.0	0.4	0.3	0.23	70	6

for forced flows. Very good agreement was obtained for the predicted (using the v^2–f model) velocity and turbulent kinetic energy profiles in wall coordinates compared with the DNS result of Kawamura (1994) for fully developed isothermal channel flow. The second and third cases demonstrated the ability of the code to simulate free convection in rectangular and cylindrical geometries. The predicted mean vertical velocity profile at the mid-height of a 5:1 aspect ratio cavity was compared with the measurements of Cheesewright et al. (1986) for $Ra = 1.6 \times 10^9$ with excellent agreement. Predicted boundary layer profiles of velocity and temperature at 90° from the bottom of a heated horizontal cylinder in free convection in air at $Ra = 1.0 \times 10^5$ were compared with the simulated results of Kuehn and Goldstein (1980). Again, there was excellent agreement and the predicted average heat transfer was within 2.4% of the result quoted by Kuehn and Goldstein.

3.3. Computational domain and boundary conditions

Experimental measurements of the cylinder heat flux made at the spanwise centerline of the test section and displaced ±0.8 and 1.6 diameters from the spanwise centerline suggested that the heat flux was nearly independent of the spanwise direction (at least near the spanwise centerline of the channel). Thus two-dimensional simulations were undertaken for the computational domain depicted in Fig. 3. The grid is constructed so that increased resolution is obtained near the surfaces of the channel and cylinder, resulting in $y^+ \leqslant 1.0$ for the first cell adjacent to these surfaces.

Application of inflow boundary conditions for the simulations differed between the unheated lower surface cases (cases 1 and 2) and the heated lower surface cases (cases 3 and 4). For the unheated lower surface cases, the experimental velocity and temperature profiles at $x = 0$ were numerically integrated and the resulting bulk velocity and temperature were specified as uniform distributions at the computational inflow boundary ($x = -300$ cm), far upstream of the heated test section. Inflow boundary conditions for the heated lower surface cases are discussed later. The upper surface was no-slip adiabatic over the entire length of the domain whereas the lower surface was no-slip adiabatic for $x < 0$ and no-slip isothermal for $x \geqslant 0$. The measured temperature distribution was set as the thermal boundary condition around the outer surface of the cylinder. An open boundary condition was utilized at the exit. Averaged values from measured profiles of velocity and temperature at the start of the test section ($x = 0$) for the cases studied are given in Table 2.

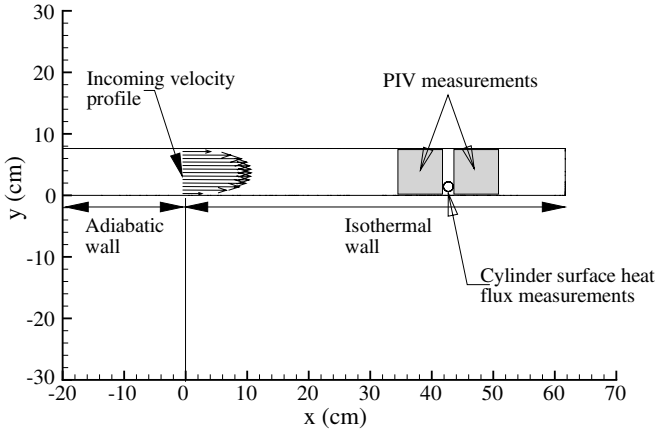

Fig. 3. Computational domain and PIV measurement locations.

4. Results

The Reynolds number based on distance from the start of the lower heated surface ($x = 0$) to the cylinder location ($x = 42$ cm) was only of order 10^4 for all cases studied; thus the inlet flow was always laminar. Furthermore, no turbulence upstream of the cylinder was detected in the experiment with lower surface heating turned off. Therefore all turbulence upstream of the cylinder can be attributed to the effects of buoyancy due to lower surface heating. In order to obtain a better understanding of the effect of the turbulent thermal plumes on the cylinder heat transfer with lower surface heating, as well as to eliminate any numerical error associated with the turbulence model, results will be presented first for cases without lower surface heating (cases 1 and 2 in Table 2) where the flow is laminar and turbulence model equations were not solved.

4.1. Laminar flow – unheated lower surface

Computed streamwise velocity profiles at $x = 0$, the start of the heated section, are compared with measurements in Fig. 4. The measured profiles are for $\overline{U}_{in} = 1.75$ (cases 1 and 3) and $\overline{U}_{in} = 1.09$ (cases 2 and 4), and there is excellent agreement between the predicted and experimental results. The velocity profiles are fairly symmetric about the centerline of the channel and demonstrate laminar developing boundary layers along both surfaces.

The computed non-dimensional temperature fields for cases 1 and 2 are presented in Fig. 5 where $T_{nd} = (T - \overline{T}_{in})/(\overline{T}_{cyl} - \overline{T}_{in})$. Note that there is no turbulence when the lower surface is unheated due to the relatively low Reynolds number. The cooled cylinder case (case 1, $Ri = 0.4$) results in unsteady separated flow in the wake whereas the heated cylinder case (case 2, $Ri = 9.1$) results in steady attached flow along the entire cylinder surface up to the plume location. The shedding sequence for the cooled cylinder case is shown in Fig. 5a–e, and the period of approximately 4 s agrees reasonably well with the shedding frequency from an isolated (no surfaces) unheated cylinder

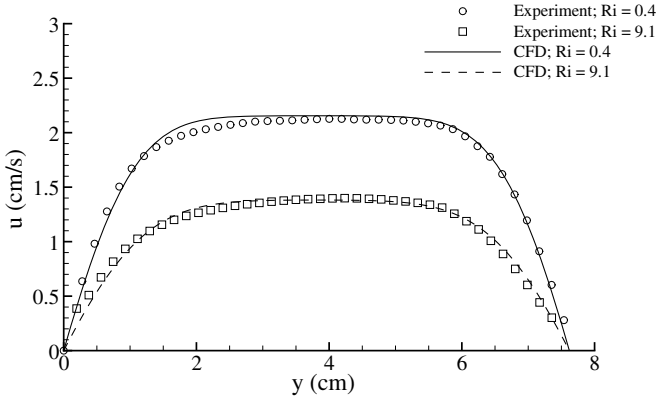

Fig. 4. Streamwise velocity profiles at $x = 0$ for case 1 and case 2 (unheated lower surface).

reported by Schlichting (1979) to be 1/4.3 s^{-1} corresponding to a Strouhal number of 0.21. The effect of buoyancy due to the heated cylinder (case 2 shown in Fig. 5f) is evident in the thermal plume coming off the upper downstream side of the cylinder (at $\theta \approx 100°$). The absence of vortex shedding in this case is consistent with the effect of buoyancy on flow patterns behind a heated cylinder in aiding forced convection (not the cross-flow studied here) noted by Chang and Sa (1989). Elimination of vortex shedding from a cylinder in cross-flow by heating the cylinder has also been shown by Lecordier et al. (1991).

The primary metric of interest is the time averaged cylinder heat transfer and Fig. 6 compares the predicted and measured time averaged heat fluxes for cases 1 and 2 (unheated lower surface). For these cases k_{turb} is zero. There is excellent agreement in both cases. For the heated cylinder case 2, there is a strong asymmetrical distribution of heat transfer around the cylinder. This might be expected due to the combined effects of buoyancy, forced flow, and cylinder location within the channel. The larger reduction in heat flux near $\theta = 100°$ for $Ri_d = 9.1$ compared with the result for $Ri_d = 0.4$ corresponds to large values of T_{nd} at the location of the plume shown in Fig. 5f.

4.1.1. Effect of gravity

The effect of buoyancy on the predicted heat flux distributions around the cylinder for cases 1 and 2 is shown in Fig. 7.

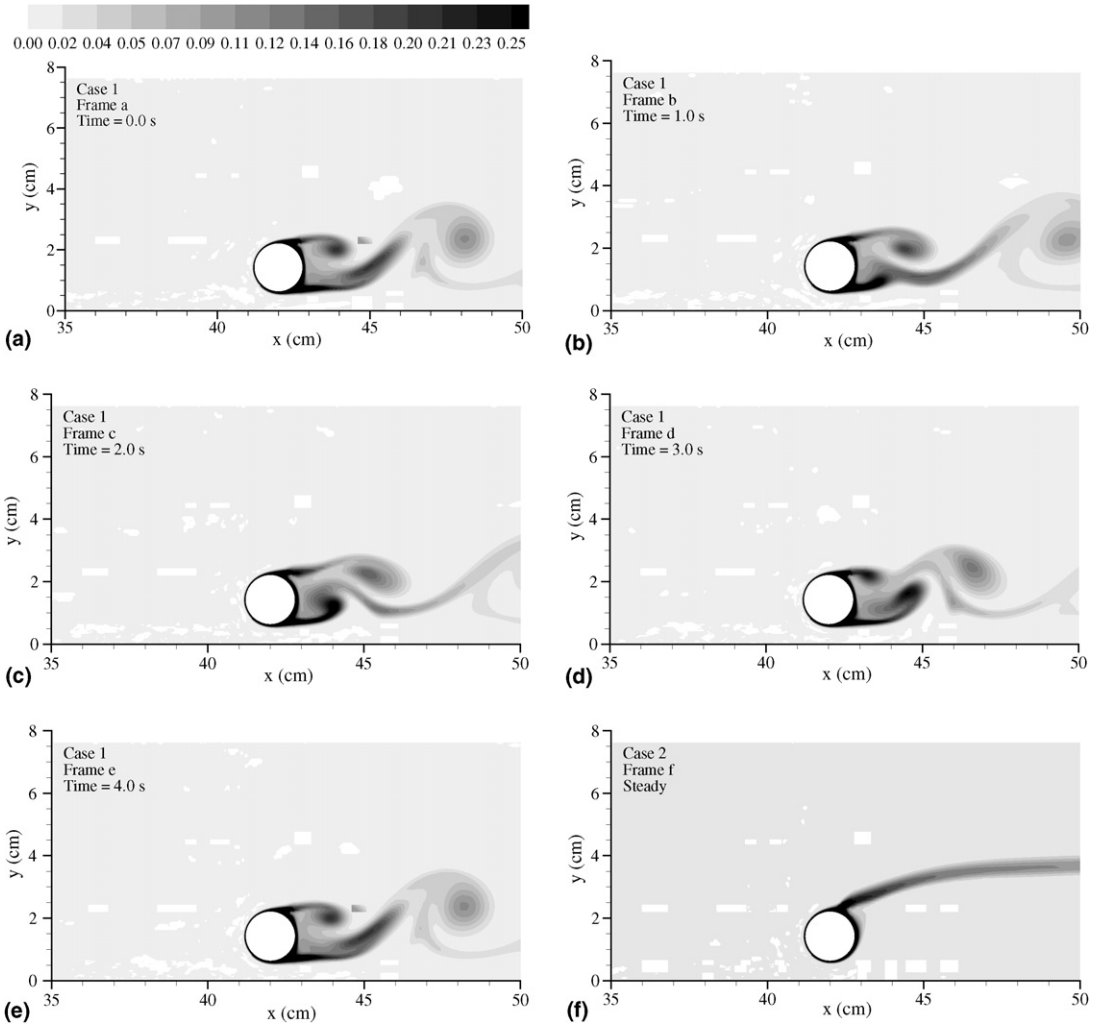

Fig. 5. Non-dimensional temperature for cooled cylinder case 1 (unsteady sequence, a–e) and heated cylinder case 2 (steady, f).

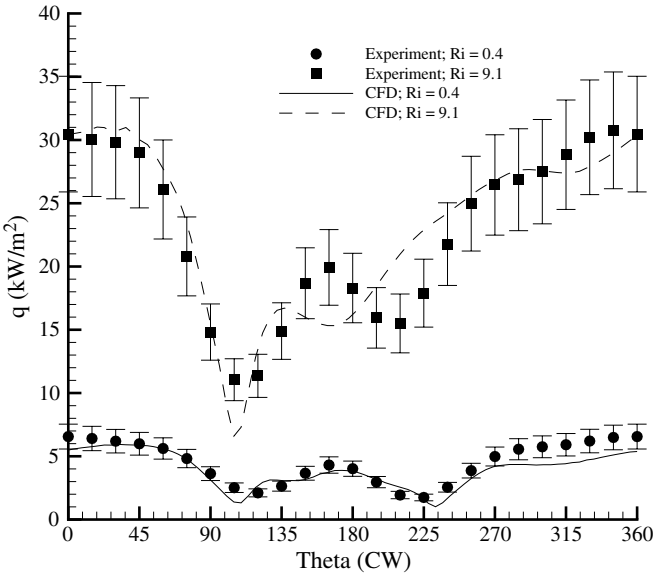

Fig. 6. Comparison of measured and predicted time average heat fluxes for cases 1 and 2 (unheated lower surface).

The absence of buoyancy is achieved numerically by setting $g = 0$ in the momentum equation and the subsequent results are referred to as case 1a and case 2a. As expected, only small differences are noted for the heat flux in the forced convection dominated case as seen in Fig. 7a. However, the mixed convection case results (Fig. 7b) now show heat flux minima in the wake region of the cylinder that are of approximately equal magnitude (when $g = 0$) as would be expected for cross-flow over an isolated cylinder in the absence of buoyancy. There are still asymmetries in the heat flux distribution due to the channel blockage factor and the proximity of the cylinder to the lower surface of the channel.

4.1.2. Effects of freestream and blockage

In order to understand the effects of the forced flow and lower surface blockage on the cylinder heat transfer, simulations were also conducted for case 1 and case 2 but with an isolated cylinder with and without a forced flow. The result is four additional cases derived from case 1 and case 2 in Table 2, namely: laminar natural convection and laminar forced convection, based on case 1 flow properties; laminar natural convection and laminar mixed convection, based on case 2 flow properties. These additional cases are referred to as case 1b, case 1c, case 2b, and case 2c, respectively. For the case of an isolated cylinder, the heat transfer to/from the cylinder results from both the difference in temperature between the cylinder surface and the surrounding fluid and the flow-field itself. The results of these simulations are shown in Fig. 8 and summarized in Table 4. Maintaining the same temperature differences as for cases 1 and 2 but turning off the forced flow results in two natural convection problems at the same Gr_d values as in the experiment. In the heated cylinder case a plume forms at $\theta = 90$ whereas in the cooled cylinder case the plume forms at $\theta = 270$. The effect of a forced flow, where U_∞ matches $\overline{U}_{in}$ of the experiment, on the heat transfer is dramatic. For example, in the cooled cylinder case, the average heat transfer increased by 80% and increased by a factor of three near the forward stagnation point. For problems where local hot spots are a concern, this is an important consideration. In the heated cylinder case (Fig. 8b), the increase of the heat transfer with the addition of forced flow is much smaller as shown in Table 4. Finally, comparing the case of an isolated (no surfaces) heated/cooled cylinder with that of a heated/cooled cylinder placed in a channel close to a lower unheated wall (i.e., the experimental geometry), the effect of blockage can be understood. There are significant differences in the distributions of the heat flux but the circumferentially averaged values are not dramatically different. Essentially, the presence of a lower surface has increased the heat transfer in both cases by approximately 10–20%.

4.2. Turbulent flow – heated lower surface

The flow entering the heated section was laminar and heating the lower surface of the channel resulted in thermal

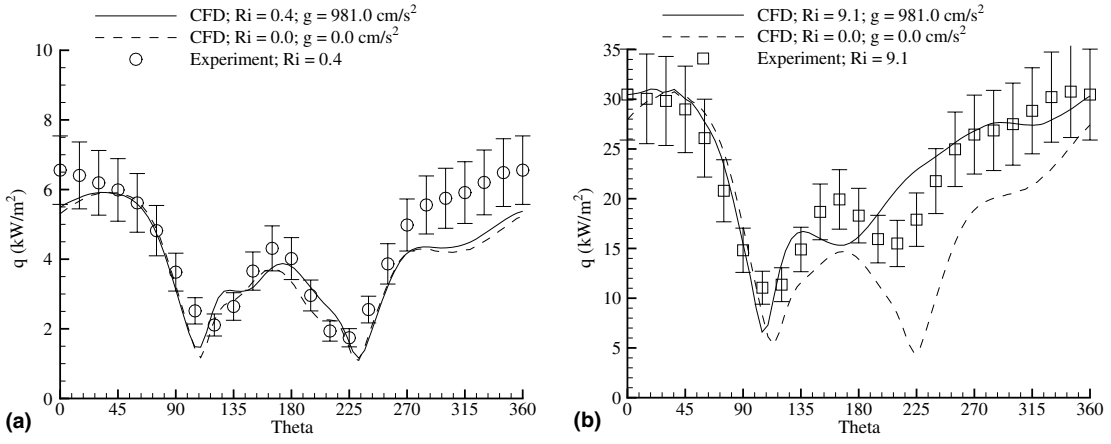

Fig. 7. Effect of buoyancy on predicted heat flux distributions around the cylinder for an unheated lower surface (a) case 1 (case 1a is for $g = 0$) and (b) case 2 (case 2a is for $g = 0$).

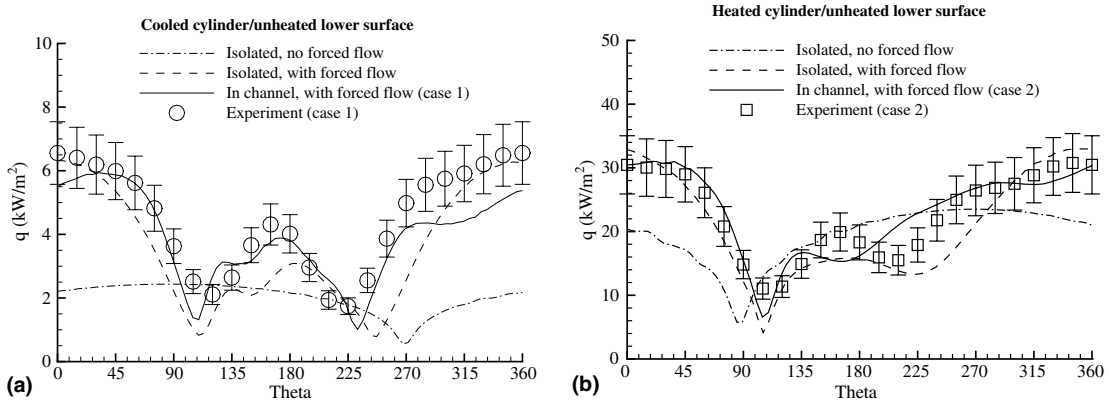

Fig. 8. Cylinder heat flux distribution demonstrating effects of blockage and forced flow for the unheated lower surface cases.

Table 4
Summary of circumferentially averaged heat flux data from Fig. 8

Cooled cylinder case	$\bar{q}$ (kW/m^2)	Heated cylinder case	$\bar{q}$ (kW/m^2)
Case 1 (experiment)	4.5	Case 2 (experiment)	22.9
Case 1 (CFD)	3.9	Case 2 (CFD)	23.1
Case 1b	2.0	Case 2b	19.4
Case 1c	3.6	Case 2c	20.8

plumes emanating from that surface which transitioned the flow from laminar to turbulent. The turbulence model described earlier was incapable of capturing this transition, resulting in very low turbulence levels and increasing plume unsteadiness upstream of the cylinder as the mesh was refined. In essence it was not possible to arrive at a grid-independent solution. To circumvent these transition-related difficulties, velocity and turbulence profiles based on the experimental measurements taken at $x = 36$ cm (5 cm upstream of the cylinder) were specified as boundary conditions at $x = 0$ for the heated lower surface simulation cases (cases 3 and 4 in Table 2). Measured profiles of the streamwise velocity, turbulent kinetic energy (where we assume $k = (2\overline{u'^2} + \overline{v'^2})/2$) and dissipation (where we assume $\varepsilon = -\overline{u'v'}\partial\overline{U}/\partial y$) at $x = 36$ cm were prescribed as boundary conditions at $x = 0$ in the simulations. A uniform temperature profile at $x = 0$ was used as the inflow thermal boundary condition since measurements of the temperature profile at $x = 36$ cm were not available. The predicted development of streamwise velocity component and turbulent kinetic energy from the inflow boundary ($x = 0$) to the location where the measurements were made ($x = 36$ cm) is shown in Fig. 9a and b, and the changes can be seen to be relatively minor. The simulations were initiated at $x = 0$ to allow for the development of the thermal boundary layer along the lower heated surface.

Four different grid levels were utilized in a grid independence study and are summarized in Table 5. The results from simulations of cases 3 and 4 using grids 1, 2 and 3 were identical everywhere except for the cylinder boundary layer. Fig. 10 shows the cylinder heat flux distribution for case 3 using the grids listed in Table 5. The very thin thermal boundary layer that develops on the cylinder requires the relatively fine meshes of either grids 3 or 4 in the wall normal direction. It was concluded that grid 4 had adequate resolution for the entire domain, including the cylinder boundary layer, and was utilized for all subsequent simulations.

Measured and predicted heat flux distributions on the cylinder for cases 3 and 4 are compared in Fig. 11. The predicted results are for $Pr_{\text{turb}} = 0.9$ and $C_{\varepsilon_4} = 1.0$, two

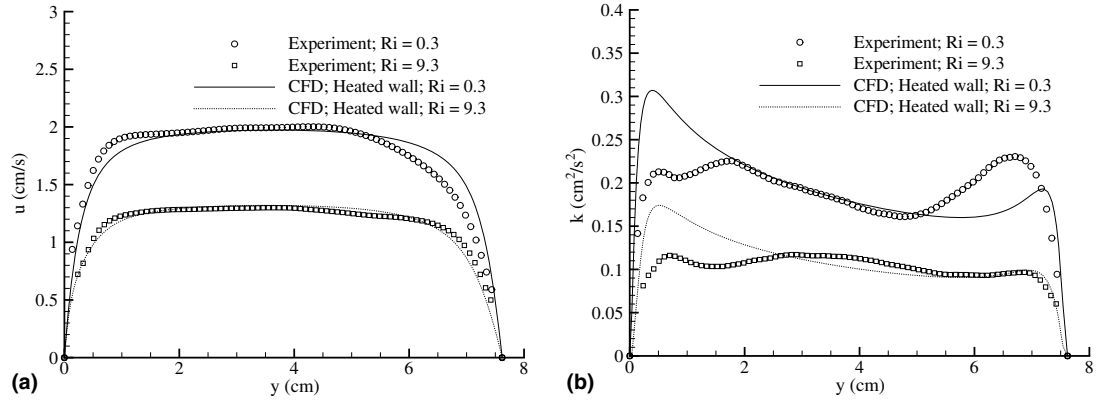

Fig. 9. Comparison of measured and predicted (a) streamwise velocity component and (b) turbulent kinetic energy profiles at $x = 36$ cm for cases 3 and 4 (heated lower surface).

Table 5
Details of the grid refinement study

	Description	Δy_{cyl} (cm)	Δy_{wall} (cm)	Number of elements
Grid 1	Coarse mesh	0.0121	0.0445	13,800
Grid 2	Grid 1 + uniform refinement	0.0061	0.0223	55,200
Grid 3	Grid 2 + uniform refinement	0.0030	0.0111	220,800
Grid 4	Grid 1 + refined annulus in wall normal direction	0.0031	0.0445	20,000

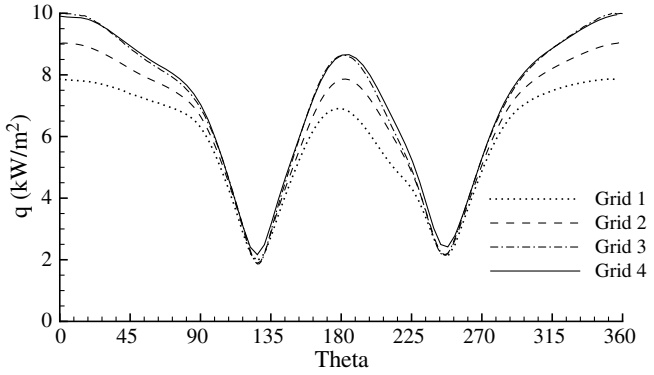

Fig. 10. The effect of grid refinement on cylinder heat flux distribution for case 3.

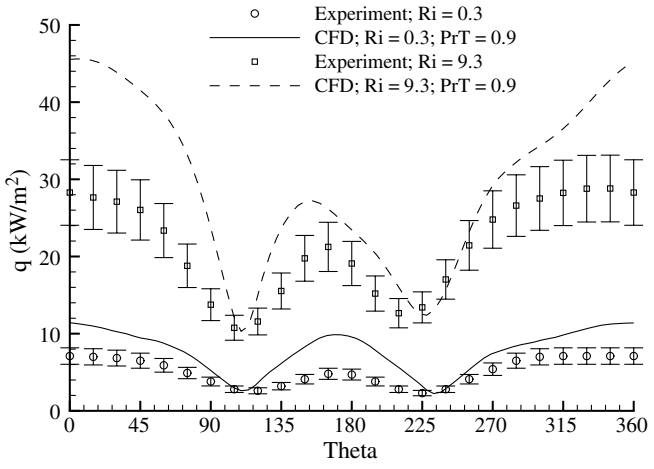

Fig. 11. Predicted and measured heat flux distributions around the cylinder for cases 3 and 4 (heated lower surface).

parameters which were found to strongly influence the simulation results. Although there is qualitative agreement for the heat flux distribution on the cylinder, the heat flux is over-predicted on the upstream side of the cylinder for both cases and on the downstream side of the cylinder for case 3 (the cooled cylinder case). This is in contrast to the very good agreement between experiment and prediction shown in Fig. 6 for cases 1 and 2 (unheated lower surface cases).

Heat transfer to or from the cylinder is dependent on the temperature of the fluid flowing over the cylinder, which depends on the heat transfer from the lower heated surface

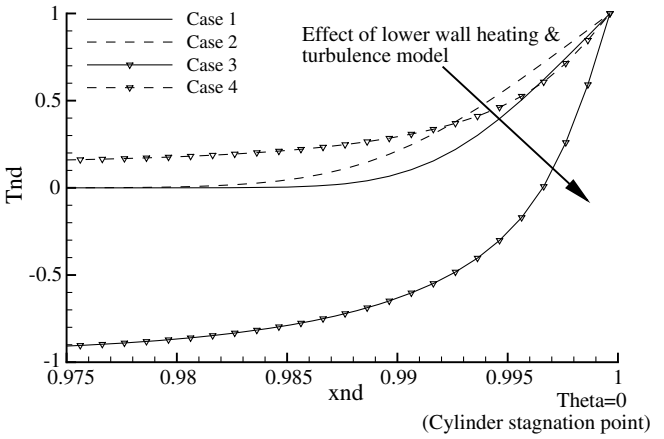

Fig. 12. Predicted normalized temperature distributions within the thermal boundary layer of the cylinder at the stagnation point ($y = 1.4269$ cm) for cases 1–4.

to the water upstream of the cylinder. This in turn depends on the details of the modeling of turbulent transport. Fig. 12 shows the predicted normalized temperature distributions within the thermal boundary layer on the cylinder along a line normal to the cylinder at the stagnation point for cases 1–4, where $x_{nd} = (x - 36)/(x_{\theta=0} - 36)$.

For cases 3 and 1 (cooled cylinder) the predicted temperature gradient at the surface of the cylinder is significantly larger for the heated lower surface case (case 3) than it for the unheated lower surface case (case 1). This larger temperature gradient would be expected to result in an increase in the cylinder heat flux compared with the unheated lower surface case result. For cases 4 and 2 (heated cylinder), however, the temperature gradient does not appear noticeably larger in Fig. 12 for the heated lower surface case (case 4) until very close to the cylinder ($x_{nd} > 0.993$).

4.2.1. Effect of turbulence parameters

Variations from the nominal values of $Pr_{turb} = 0.9$ and $C_{\varepsilon_4} = 1.0$ were found to significantly alter the turbulent flowfield and consequently the cylinder heat flux predictions. A parameter study that varied C_{ε_4} showed that smaller values resulted in reduced production of ε and large k values near the lower heated surface and also larger cylinder heat flux. The sensitivity of the cylinder heat flux to Pr_{turb} is shown in Fig. 13 where increasing Pr_{turb} by 60% to 1.45 results in reduced cylinder heat flux by up to 30% in the stagnation region for the cooled cylinder case (case 3) and in the wake region for the heated cylinder case (case 4). This is because increasing Pr_{turb} reduces the production of both k and ε. Based on DNS data for stratified flows, Pr_{turb} up to 1.4 has been suggested and used in RANS modeling of buoyant flows (Venayagamoorthy et al., 2003).

4.3. Average Nusselt numbers

Circumferentially averaged Nusselt numbers for the computations and experiments are listed in Table 6. The

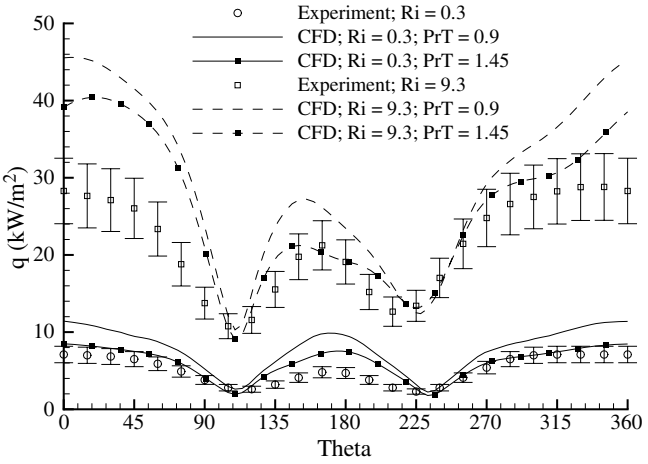

Fig. 13. Effect of turbulent Prandtl number on cylinder heat flux predictions for cases 3 (cooled cylinder) and 4 (heated cylinder).

Table 6
Circumferentially averaged cylinder Nusselt numbers

Cylinder cases with channel	$\overline{Nu}$ (simulation)	$\overline{Nu}$ (experiment)	Relative difference (%)
Case 1	22.2	25.6	13.3
Case 2	21.9	21.8	0.5
Case 3	60.9	39.9	52.6
Case 4	27.3	19.9	37.2
Case 1a ($g = 0$)	22.5	–	–
Case 2a ($g = 0$)	17.4	–	–
Case 3 ($Pr_{turb} = 1.45$)	47.3	–	18.6
Case 4 ($Pr_{turb} = 1.45$)	24.1	–	4.4

computed Nusselt number is based on the time averaged heat flux, temperature difference $(\overline{T}_{cyl} - \overline{T}_{in})$, and material properties evaluated at the film temperature $(\overline{T}_{in} + \overline{T}_{cyl})/2$. The agreement is very good and within the experimental uncertainty of ±15% for the unheated lower surface cases (laminar flow cases 1 and 2). However, for the nominal turbulence parameter values, the predicted $\overline{Nu}$ for the heated lower surface cases (turbulent flow cases 3 and 4) are 53% and 37% larger, respectively, than the measured $\overline{Nu}$. In case 3 the difference between the water temperature at the inlet of the channel and the average cylinder temperature is only 3.4 K; thus a small error in either measured or computed temperature can result in a large error in $\overline{Nu}$. For the cooled cylinder case, heating of the lower surface results in a large increase in $\overline{Nu}$, 56% in the experiment and 174% in the simulation. For the heated cylinder case, lower surface heating produces a decrease in $\overline{Nu}$ of 9% in the experiment and an increase of 25% in the simulation. Increasing Pr_{turb} to 1.45 improves the agreement between experimental and computed $\overline{Nu}$ to essentially within the uncertainty of the measurements.

Correlations of cylinder heat transfer in cross-flow are primarily for an isolated cylinder (without channel surfaces). This is in contrast to the present study which has a geometry with heated or unheated channel surfaces in close proximity to the cylinder as considered in cases 1–4. To provide additional validation of the numerical work, average cylinder Nusselt numbers were determined from the results of the simulations performed for an isolated cylinder (without channel surfaces) that were discussed in Section 4.1.2 and summarized in Table 4. These average (isolated) Nusselt numbers are compared with correlations from the literature in Table 7 and designated as cases 1b, 1c and cases 2b, 2c.

Table 7
Circumferentially averaged cylinder Nusselt numbers: comparisons of results from calculations without channel surfaces with results of correlations

Cylinder cases without channel (isolated)	$\overline{Nu}$ (simulation)	$\overline{Nu}$ (correlation)	Relative difference (%)
Case 1b ($U_{in} = 0$; laminar natural convection)	11.3	10.1	11.9
Case 1c ($U_{in} \neq 0$; laminar forced convection)	20.4	19.1	6.8
Case 2b ($U_{in} = 0$; laminar natural convection)	18.4	18.3	0.5
Case 2c ($U_{in} \neq 0$; laminar mixed convection)	19.8	19.0	4.2

The correlation of Churchill and Bernstein (1977) for forced convection from an isolated cylinder subject to a flow normal to the cylinder axis

$$\overline{Nu} = 0.3 + 0.62Re^{1/2}Pr^{1/3}/[1 + (0.4/Pr)^{2/3}]^{1/4} \quad (4)$$

was used to determine the forced convection component of the correlation values reported in Table 7. Fluid properties are evaluated at the film temperature. For the cases without flow (case 1b and case 2b in Table 7), and for the free convection component of the Nusselt number correlation for the cases with flow (case 1c and case 2c in Table 7), Morgan's (1975) correlation for the average Nusselt number in laminar natural convection from a heated horizontal cylinder

$$\overline{Nu}_{natural} = 0.48(Gr_d Pr)^{1/4} \quad (5)$$

was used. For case 2c, the combining rule correlation of Oosthuizen and Naylor (1999) for mixed convection heat transfer from a horizontal cylinder in cross-flow

$$\overline{Nu}^7 = \overline{Nu}^7_{forced} + \overline{Nu}^7_{natural} \quad (6)$$

was used. The calculated Nusselt numbers are in good agreement with the correlations, with the maximum difference being less than 12% for the case of natural convection from a cooled cylinder. These results provide additional verification for the numerical results presented in this work.

5. Conclusions

Heat transfer to/from a cooled/heated horizontal circular cylinder in a cross-flow of water was studied both numerically and experimentally. The cylinder was placed near the lower surface of a water channel. The water

flowing into the test section was laminar and the lower surface temperature of the channel was controlled, giving rise to either laminar or turbulent mixed or forced convection heat transfer to or from the cylinder. When the lower surface temperature matched the inflow water temperature the flow was laminar and for both mixed and forced convection the numerical and experimental heat flux distributions around the cylinder circumference were in excellent agreement. In particular, the average cylinder surface Nusselt number was well within the experimental uncertainty for both the mixed and forced convection cases. The effects of gravity, forced flow and blockage on the cylinder heat transfer were studied numerically.

When the lower surface temperature was increased, turbulent thermal plumes and the transition from laminar forced to turbulent mixed convection proved difficult to model with the v^2–f turbulence model and SGDH to account for production of turbulent kinetic energy due to buoyancy. Two important parameters were identified regarding the modeling of the turbulence, namely the turbulent Prandtl number, Pr_{turb}, and C_{ε_4}, the coefficient controlling production of dissipation due to buoyancy in the SGDH implementation. In particular, increasing the turbulent Prandtl number by 60% reduced the average Nusselt number difference between the experiment and computations by nearly 30% to within experimental uncertainty.

Acknowledgement

This work was supported within Sandia National Laboratories as a verification and validation activity and is part of a larger DOE ASC program. The authors are appreciative of numerous fruitful communications with Paul Durbin and Sheldon Tieszen regarding turbulence modeling issues as well as code implementation support from Stefan Domino, Chris Moen, and Greg Wagner.

Appendix A. Solution of 2D conduction problem on the cylinder-wall domain

The heat flux distribution along the outer cylinder surface was determined via the solution of a two-dimensional conduction problem:

$$\frac{1}{r}\frac{\partial}{\partial r}\left(r\frac{\partial T}{\partial r}\right)+\frac{1}{r^2}\frac{\partial^2 T}{\partial \theta^2}=0 \quad r_i \leqslant r \leqslant r_0;\ \ 0 \leqslant \theta < 2\pi;$$

$$T(r=r_0,\theta)=T_0(\theta) \tag{A.1}$$

$$-k\frac{\partial T}{\partial r}(r=r_i,\theta)=h[T_i-T(r=r_i,\theta)];$$

$$T(r,\theta=0)=T(r,\theta=2\pi),\quad \frac{\partial T}{\partial \theta}(r,\theta=0)=\frac{\partial T}{\partial \theta}(r,\theta=2\pi) \tag{A.2}$$

The outer-surface boundary condition, $T_0(\theta)$, in Eq. (A.1) is the measured outer cylinder surface temperature profile. The mixed boundary condition in Eq. (A.2) represents heat transfer from the inner cylinder tube wall to cooling/heating water flow supplied to the tube-side of the test cylinder. The measured tube-side water flow and temperature were used to calculate the convective heat-transfer coefficient, h, using the Dittus and Boelter (1930) correlation for fully developed turbulent flow in a tube. The temperature, T_i, of the tube-side water flow was measured with thermocouples at the entrance and exit of the test-cylinder tube. The water flow rate through the cylinder was sufficiently high to minimize axial temperature variations.

The solution to Eqs. (A.1) and (A.2) was found using a separation of variables approach. The solution is applicable for steady-state conduction in a constant-conductivity annulus with an arbitrary outer surface temperature profile and a mixed convective–conductive boundary condition at the inner surface. The Fourier-series solution for the tube-wall temperature distribution is written as:

$$T(r,\theta)=\frac{T_i-\overline{T_0}}{\ln\frac{r_i}{r_0}-\frac{k}{hr_i}}\ln\frac{r}{r_0}+\sum_{n=1}^{\infty}\left(C_n(r)\frac{G_n}{F_n}+\frac{D_n(r)}{R_n}\right)(a_n\sin n\theta+b_n\cos n\theta) \tag{A.3}$$

where $\overline{T_0}$ is the mean of the outer surface thermocouple data. The heat flux at the outer tube wall, which was the primary metric of interest for the simulation studies, was obtained by differentiating the solution and applying Fourier's law:

$$q''(\theta)=-k\left.\frac{\partial T}{\partial r}\right|_{r=r_0}=-k\frac{T_i-\overline{T_0}}{\ln\frac{r_i}{r_0}-\frac{k}{hr_i}}\frac{1}{r_0}-\lambda\sum_{n=1}^{\infty}\left(C_n'(r_0)\frac{G_n}{F_n}+\frac{D_n'(r_0)}{R_n}\right)(a_n\sin n\theta+b_n\cos n\theta) \tag{A.4}$$

where the following definitions apply:

$$a_n=\frac{1}{\pi}\int_0^{2\pi}T_0(\theta)\sin n\theta\,\mathrm{d}\theta;\quad b_n=\frac{1}{\pi}\int_0^{2\pi}T_0(\theta)\cos n\theta\,\mathrm{d}\theta \tag{A.5}$$

$$C_n(r)=r^n-\frac{r_0^{2n}}{r^n};\quad C_n'(r_0)=2nr_0^{n-1} \tag{A.6}$$

$$G_n=\frac{2}{\left(\frac{r_i}{r_0}\right)^n+\left(\frac{r_0}{r_i}\right)^n};\quad F_n=\frac{nk}{h}\left(r_i^{n-1}+\frac{r_0^{2n}}{r_i^{n+1}}\right)+\frac{r_0^{2n}}{r_i^n}-r_i^n \tag{A.7}$$

$$D_n(r)=\frac{r^n}{r_i^{2n}}+r^{-n};\quad D_n'(r_0)=n\left(\frac{r_0^{n-1}}{r_i^{2n}}-r_0^{-(n+1)}\right) \tag{A.8}$$

$$R_n=\frac{r_0^n}{r_i^{2n}}+r_0^{-n} \tag{A.9}$$

References

Abdelmeguid, A.M., Spalding, D.B., 1979. Turbulent flow and heat transfer in pipes with buoyancy effects. J. Fluid Mech. 94 (2), 383–400.

Abu-Mulaweh, H.I., Chen, T.S., Armaly, B.F., 2000. Effects of free-stream velocity on turbulent natural-convection flow along a vertical plate. Exp. Heat Transfer 13, 183–195.

Abu-Mulaweh, H.I., Armaly, B.F., Chen, T.S., 2001. Turbulent mixed convection flow over a backward-facing step. Int. J. Heat Mass Transfer 44 (14), 2661–2669.

Afshari, B., 1989. Computation of three-dimensional turbulent-mixed convection boundary layers. PhD Thesis, Stanford University.

Aicher, T., Martin, H., 1997. New correlations for mixed turbulent natural and forced convection heat transfer in vertical tubes. Int. J. Heat Mass Transfer 40 (15), 3617–3626.

Baliga, B.R., Patankar, S.V., 1983. A control volume finite-element method for two-dimensional fluid flow and heat transfer. Numer. Heat Transfer 6 (3), 245–261.

Chang, K.-S., Sa, J.-Y., 1989. Numerical study of the unsteady mixed convection heat transfer from a circular cylinder. Int. Commun. Heat Mass Transfer 16, 427–434.

Cheesewright, R., King, K.J., Ziai, S., 1986. Experimental data for the validation of computer codes for the prediction of two-dimensional buoyant cavity flow. In: Proceeding of the ASME Meeting, HTD, vol. 60, pp. 75–81.

Chen, T.S., Armaly, B.F., Ali, M.N., 1987. Turbulent mixed convection along a vertical plate. J. Heat Transfer 109 (1), 251–253.

Cheng, K.C., Obata, T., Gilpin, R.R., 1986. Buoyancy effects on forced convection heat transfer in the transition regime of a horizontal boundary layer from below. In: ASME Paper 86-WA/HT-97, Presented at Winter Annual Meeting, Anaheim, CA, December 7–12.

Churchill, S.W., Bernstein, M., 1977. A correlating equation for forced convection from gases and liquids to a circular cylinder in crossflow. J. Heat Transfer 99, 300–306.

Cotton, M.A., Jackson, J.D., 1990. Vertical tube air flows in the turbulent mixed convection regime calculated using a low-Reynolds-number k–ε model. Int. J. Heat Mass Transfer 33 (2), 275–286.

Dittus, F.W., Boelter, L.M.K., 1930. University of California Publications on Engineering, vol. 2, p. 443.

Durbin, P.A., 1991. Near-wall turbulence closure modeling without 'damping functions'. Theoret. Comput. Fluid Dyn. 3, 1–13.

Evans, G., Greif, R., Siebers, D., Tieszen, S., 2005. Turbulent mixed convection from a large, high temperature, vertical flat surface. Int. J. Heat Fluid Flow 26, 1–11.

Fand, R.M., Keswani, K.K., 1973. Combined natural and forced convection heat transfer from horizontal cylinders to water. Int. J. Heat Mass Transfer 16, 1175–1191.

Hattori, Y., Tsuji, T., Nagano, Y., Tanaka, N., 2000. Characteristics of turbulent combined-convection boundary layer along a vertical heated plate. Int. J. Heat Fluid Flow 21, 520–525.

Hattori, Y., Tsuji, T., Nagano, Y., Tanaka, N., 2001. Effects of freestream on turbulent combined-convection boundary layer along a vertical heated plate. Int. J. Heat Fluid Flow 22, 315–322.

Humphrey, J.A.C., To, W.M., 1986. Numerical simulation of buoyant turbulent flow – II. Free and mixed convection in heated cavities. Int. J. Heat Mass Transfer 29 (4), 593–610.

Imura, H., Gilpin, R.R., Cheng, K.C., 1978. An experimental investigation of heat transfer and buoyancy induced transition from laminar forced convection to turbulent free convection over a horizontal isothermally heated plate. J. Heat Transfer 100, 429–434.

Jackson, J.D., Cotton, M.A., Axcell, B.P., 1989. Studies of mixed convection in vertical tubes. Int. J. Heat Fluid Flow 10 (1), 2–15.

Joye, D.D., Bushinsky, J.P., Saylor, P.E., 1989. Mixed convection heat transfer at high Grashof number in a vertical tube. I&EC Res. 28, 1899–1903.

Kalitzin, G., 1999. Application of the v^2–f model to aerospace configurations. CTR Annu. Res. Briefs, 289–300.

Kawamura, H., 1994. Direct numerical simulation of turbulence by finite difference scheme. The recent developments in turbulence research. In: Proceedings of the SINO-JAPAN Workshop of Turbulent Flows. International Academic Publishers, Beijing, pp. 54–60.

Kearney, S.P., Grasser, T.W., Liter, S.G., Evans, G.H., Greif, R., 2005. Experimental investigation of a cylinder in turbulent thermal convection with an imposed shear flow. AIAA Paper 2005-1124.

Kieft, R.N., Rindt, C.C.M., van Steenhoven, A.A., 1999. The wake behaviour behind a heated horizontal cylinder. Exp. Therm. Fluid Sci. 19, 183–193.

Kitamura, K., Inagaki, T., 1987. Turbulent heat and momentum transfer of combined forced and natural convection along a vertical flat plate—aiding flow. Int. J. Heat Mass Transfer 30 (1), 23–41.

Kuehn, T.H., Goldstein, R.J., 1980. Numerical solution to the Navier–Stokes equations for laminar natural convection about a horizontal circular cylinder. Int. J. Heat Mass Transfer 23, 971–979.

Lecordier, J.C., Hamma, L., Paranthoen, P., 1991. The control of vortex shedding behind heated circular cylinders at low Reynolds number. Exp. Fluids 10, 224–229.

Lei, C., Cheng, L., Kavanagh, K., 2001. Spanwise length effects on three-dimensional modeling of flow over a circular cylinder. Comput. Methods Appl. Mech. Eng. 190, 2909–2923.

Li, A., Zhao, J.Z., Chen, T.S., Armaly, B.F., 1998. The effect of forced flow on turbulent natural convection adjacent to a vertical backward-facing step. In: Heat Transfer 1998, Proc. 11th Int. Heat Transfer Conf., August 23–28, Kyongju, Korea, vol. 3, pp. 269–274.

Lin, S.-J., Churchill, S.W., 1978. Turbulent free convection from a vertical, isothermal plate. Numer. Heat Transfer 1, 129–145.

Lowery, G.W., Vachon, R.I., 1975. The effect of turbulence on heat transfer from heated cylinders. Int. J. Heat Mass Transfer 18, 1229–1242.

Moen, C.D., Evans, G.H., Domino, S.P., Burns, S.P., 2002. A multi-mechanics approach to computational heat transfer. In: IMECE2002-33098, Proc. 2002 ASME Int. Mechanical Eng. Congress and Exhibition, New Orleans, November 17–22.

Morgan, V.T., 1975. The overall convective heat transfer from smooth circular cylinders. In: Irvine, T.F., Hartnett, J.P. (Eds.), Advances in Heat Transfer, vol. 11. Academic Press, New York, pp. 199–264.

Nakos, J.T., Keltner, N.R., February 1989. The radiative–convective partitioning of heat transfer to objects in large pool fires, Sandia National Laboratories Report SAND89-0360C.

Oosthuizen, P.H., Madan, S., 1970. Combined convective heat transfer from horizontal cylinders in air. J. Heat Transfer (February), 194–196.

Oosthuizen, P.H., Naylor, D., 1999. Introduction to Convective Heat Transfer Analysis. WCB/McGraw-Hill.

Patel, K., Armaly, B.F., Chen, T.S., 1998. Transition from turbulent natural to turbulent forced convection. J. Heat Transfer 120 (November), 1086–1089.

Plumb, O.A., Evans, G.H., 1983. Turbulent mixed convection from a vertical heated surface in a crossflow. In: Proc. ASME-JSME Thermal Eng. Joint Conf., Honolulu, Hawaii, March 20–24, vol. 3, pp. 47–53.

Ramachandran, N., Armaly, B.F., Chen, T.S., 1990. Turbulent mixed convection over an isothermal horizontal flat-plate. J. Heat Transfer 112 (1), 124–129.

Rodi, W., Hossain, M.S., 1982. A turbulence model for buoyant flow and its application to vertical buoyant jets. In: Rodi, W. (Ed.), HMT, The Science and Applications of Heat and Mass Transfer, vol. 6. Pergamon Press.

Schlichting, H., 1979. Boundary Layer Theory, seventh ed. McGraw-Hill, New York.

Schneider, G.E., Raw, M.J., 1986. A skewed, positive influence coefficient upwinding procedure for control-volume-based finite-element convection–diffusion computation. Numer. Heat Transfer 9 (1), 1–26.

Siebers, D.L., Schwind, R.G., Moffat, R.F., 1982. Experimental mixed convection from a large, vertical plate in a horizontal flow. In: Paper MC13, 3, Proc. 7th Int. Heat Transfer Conf., Munich.

Sveningsson, A., 2003. Analysis of the performance of different v^2–f turbulence models in a stator vane passage flow, PhD Thesis, Chalmers University of Technology.

van Steenhoven, A.A., Rindt, C.C.M., 2003. Flow transition behind a heated cylinder. Int. J. Heat Fluid Flow 24, 322–333.

Venayagamoorthy, S.K., Koseff, J.R., Ferziger, J.H., Shih, L.H., 2003. Testing of RANS turbulence models for stratified flows based on DNS data. CTR Ann. Res. Briefs 2003, 127–138.

Williamson, C.H.K., 1996. Vortex dynamics in the cylinder wake. Annu. Rev. Fluid Mech. 28, 477–539.

Zhukauskas, A., Ziugzda, J., 1985. Heat Transfer of a Cylinder in Crossflow. Hemisphere Publishing Corporation.